International Journal of Medical, Medicine and Health Sciences
ISSN: 2517-9969
Vol:5, No:1, 2011

Real-time Haptic Modeling and Simulation for Prosthetic Insertion

Catherine A. Todd and Fazel Naghdy

***Abstract*—**In this work a surgical simulator is produced which enables a training otologist to conduct a virtual, real-time prosthetic insertion. The simulator provides the Ear, Nose and Throat surgeon with real-time visual and haptic responses during virtual cochlear implantation into a 3D model of the human Scala Tympani (ST). The parametric model is derived from measured data as published in the literature and accounts for human morphological variance, such as differences in cochlear shape, enabling patient-specific pre- operative assessment. Haptic modeling techniques use real physical data and insertion force measurements, to develop a force model which mimics the physical behavior of an implant as it collides with the ST walls during an insertion. Output force profiles are acquired from the insertion studies conducted in the work, to validate the haptic model. The simulator provides the user with real-time, quantitative insertion force information and associated electrode position as user inserts the virtual implant into the ST model. The information provided by this study may also be of use to implant manufacturers for design enhancements as well as for training specialists in optimal force administration, using the simulator. The paper reports on the methods for anatomical modeling and haptic algorithm development, with focus on simulator design, development, optimization and validation. The techniques may be transferrable to other medical applications that involve prosthetic device insertions where user vision is obstructed.

***Keywords*—**Haptic modeling, medical device insertion, real-time visualization of prosthetic implantation, surgical simulation.

I. Introduction

SURGICAL simulators offering the user force-feedback as well as visual cues for real-time control have potential for use in pre-operative planning and medical training. Due to technological advances in computer processing speed and the development of customizable haptic devices and supporting software, the development of more realistic anatomical models that have real-world properties is apparent. Highly invasive medical procedures can now be replicated in a virtual environment where complex scenarios can be repeated for surgeon training without putting the patient at risk. Further, it enables objective evaluation surgeon technique as well as analysis of device behavior.

Force feedback extends the experience for the simulator user, providing them with a heightened sense of immersion into the Virtual Environment (VE) than that of experiencing only visual stimuli. Touch sensation is a vital information channel for humans in real-world scenarios; particularly for surgeons which use delicate equipment to interact with the delicate structures of the human body.

Cochlear implantation is an intrusive procedure. Prior to insertion of the Cochlear Implant (CI), the surgeon accesses the cochlear Round Window (RW) by performing a mastoidectomy (temporal bone drilling), which is followed by a cochleostomy (opening the cochlea for CI insertion). The Ear, Nose and Throat (ENT) surgeon uses forceps to grasp the electrode carrier end and advance it into the ST. For the Standard Insertion Technique (SIT), the straightening stylet is removed when the electrode is at full insertion depth. Connective tissue is placed about the cochleostomy site to seal it and avoid post-operative CI slippage. Throughout this process there is risk of inducing trauma or loss of motor-sensory function to the delicate structures that reside between the external and inner ear, and within the cochlear itself. Anatomy in this region varies between patients, such as in the size and shape of the structures and clinical anomalies makes this difference even more profound. The negotiation of traversing this region is therefore a difficult process, however it is an important one since results of patient hearing post-device insertion and after rehabilitation may be improved by optimal implant positioning close to the modiolus, orientation toward the modiolus and appropriate force administration.

During the CI insertion, the implant disappears out of surgeon view soon after initial advancement past the cochleostomy site, around the region of the Basal turn. The surgeon then relies on sense of touch for the rest of the insertion. Excess pressure after the first point of resistance may lead to induced trauma to the Cochlear Partition (CP). Force feedback is required during this intricate process to minimize the risk of avoidable damage to the cochlea. Force rendering is therefore vital to accurately relay information associated with device/structure interactions for this surgical procedure.

Force rendering has been applied for temporal bone drilling simulations [1], [2], [3], [4], [5], [6], [7], soft tissue palpations [8], [9], [10], [11], [12], [13] and device insertions such as needle insertions [14], [15], [16], [17], [18], [19] for spine biopsy [15], neurosurgery [20] and lower back puncturing [21]. Virtual routines also include needle insertions for prostate cancer diagnosis [9] and treatment [17], catheter insertions [16], [22], [23], [24], human thigh [25] and knees examinations [18], endoscopies [7], [26], laparoscopies [27], [28], [29], [30], [31], [32] for bile duct exploration [28], gall bladder removals [28], [30] and abdominal surgery [33].

C. A. Todd is with the Faculty of Computer Science and Engineering, University of Wollongong in Dubai, PO 20183, UAE (phone: 971-4-367-2432; fax: 971-4-3672670; e-mail: catherinetodd@uowdubai.ac.ae).

F. Naghdy is with University of Wollongong, Wollongong, NSW, 2512, Australia (e-mail: fazel@uow.edu.au).

Haptic models may involve multiple or single -point collisions, proxy-based methods and use surface representations or volume renderings. There are no existing simulators for cochlear implantation that offer force feedback during a real-time, virtual CI insertion. Some animations of this process exist which use 3D cochlear reconstructions, as reported in [34] and [35], however the cochlea is modeled as a single chamber and as such, the path for implant trajectory is non-realistic, since the ST chamber of the cochlea is the primary passage for CI insertion. In this work a real-time, interactive surgical simulator that offers force feedback is produced, which uses a 3D model of the human ST, for CI device insertions.

II. Method

A. Insertion Force Measurement

Force administration and electrode trajectories were evaluated via experimentation for the Nucleus® 24 Contour™ CI, using the Standard Insertion Technique (SIT). The experimentation was conducted for the purpose of replication of the procedure within the VE and for simulator validation. Experimental results include insertion force profiles and coefficient of friction measurement between the electrode/ST interface. The experimental rig comprised of an Instron 5543 force measurement device with a 10N load cell (Fig. 1) was used to collect insertion force data and associated distance along the cochlea as the Contour electrode was advanced into a synthetic ST model. Since insertion forces are principally encountered along the longitudinal length of the electrode, the 2D model sufficed for insertion force data analysis.

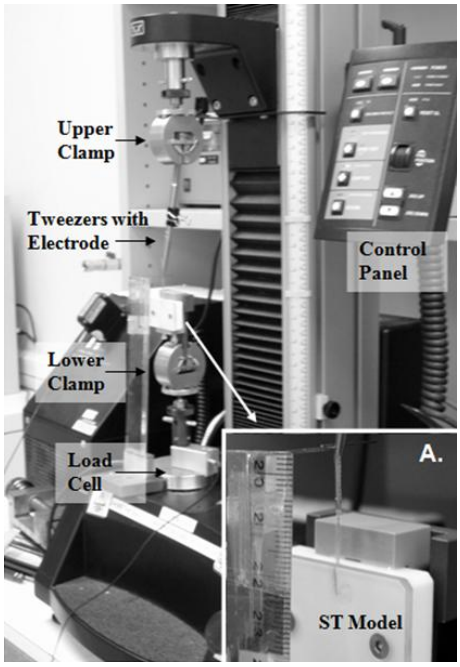

Fig. 1 Experimental Rig for Measurement of Insertion Forces

A soap solution was applied to the ST chamber prior to each electrode insertion. Further, the stylet and silicone carrier were straightened carefully to their pre-curled state, and the stylet reinserted, using a specialized device for this purpose, provided by Cochlear™, in between replications. The electrode was attached to tweezers, held by a clamp, as the apparatus was advanced at a constant speed of 120mm/min, until the electrode reached a full insertion depth (the second rib of the carrier was at the passage opening), inside the ST cavity (held stationary in a clamp). The stylet was then withdrawn. During this process insertion forces were measured by the load cell at 50ms sample intervals and the data is logged to the PC. This procedure was repeated several times. To prevent spikes in the force profile due to the silicone tip catching at the ST entrance, the advancement of the electrode commenced with the tip placed an initial 1-3mm inside the ST entrance. Force profiles are plotted from the logged data and used for simulator validation (Results section).

B. Cochlear Modeling

The human cochlea is a tiny 3D spiral, comprised of three fluid-filled chambers: the Scala Tympani (ST), the Scala Vestibuli (SV) and the Scala Media (SM) which separates the former two. The ST is the primary passage for CI insertion and as such, is modeled in this work for the purpose of virtual implantation. Since segmentation of this structure is not possible from spiral CT, measured data as reported in [36], [37], [38], [39], [40], [41] are considered for the design and construction of the ST model.

ST cross-sectional data including cross-section area, ST width and ST height as documented in [41] were plotted at each quarter turn, along the length of the cochlea: from 0mm to 35.58mm [38]. At each of these quarter turn cross-sections, values for cochlear radii [37] and ST percentage lengths [38] are combined to give a value for the distance of the cochlear Inner Wall (IW) from the modiolar axis. Measurements for ST Outer Wall (OW) and IW data [37], [38] were then combined with cochlear diameters at each cochlear half turn [36], [39], and given as a function of angular displacement.

The Basilar Membrane (BM) rests on the inferior edge of the SM; separating this chamber from the superior wall of the ST and is approximated as a flat structure, increasing linearly in width from 0.15mm at the RW to 0.52mm at its apical end [40]. The BM inner edge is located at the center of the ST cross-section [36] and the ST sides are approximated by parabolas. The site of the RW is the start of the model spiral, at an angular displacement of 13.47° [37]. From this location, the cross-sections are defined at each quarter turn, and at the apex.

Variation in cochlear height information is considered [9], [35], [36] to extend the spiral into 3D. Cochlear height typically increases as the cochlea spirals from base to apex with change in axial height from 1.93mm to 4mm [36], [9] and intra-cochlear tilt [35], [36]. Combining this height data, a constant height increase of 10° is introduced to the model and with intra-cochlear tilt variations after the first turn to give a total axial height of 2.56mm, which is close to the average; 2.75mm [36]. The final spiral approximation compared well with measured data [41].

The spiral model derived from the measured data is then parameterized to provide a patient-specific model of the human ST, which captures morphological variation. This parametric model is produced by representing each quarter turn cross-section height and width as percentages of the initial cross-section, as defined at the RW location. Distance values from the modiolus to the ST IW at each cross-section are computed as percentages of Organ of Corti (OC) length. These approximations of the cross-sections at each quarter turn may be obtained from three parameters: ST length, and width and height of the first (RW) cross-section. The data can be obtained from CT scans, which are taken pre-operatively to determine CI candidacy. A Finite Element (FE) model is produced in ANSYS (Fig. 2) using this approach. The FE model was validated by comparison with measured data from the literature reported previously and mathematical reconstructions including the helico-spiral approximation [35] and the Archimedian spiral [36]. The FE surface model will be used in the virtual CI surgical suite, described in the next section of work.

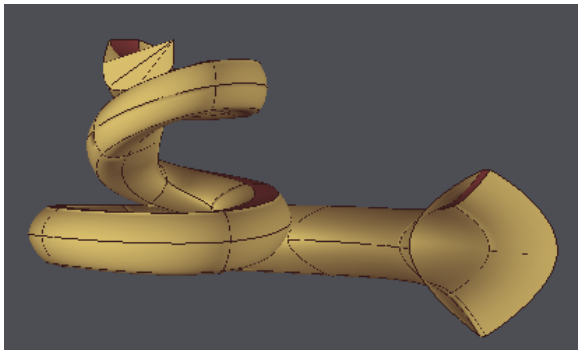

Fig. 2 Parametric FE Model of the human ST

C. Scene Rendering

Visual and haptic rendering algorithms enabling real-time interactions between the virtual CI and FE surface model were implemented in C++, VRML and Python, within the Reachin Application Programming Interface (API), interfaced to a Phantom 6DOF haptic device (SensAble Technologies). Scene graph nodes were constructed and defined in VRML; containing the surface model data and associated attributes (such as color, normals, vertex location). Python script was used for field event handling, enabling movement of objects within the scene linked with user-initiated manipulation. Crystal Eyes provided the user with stereoscopic viewing, giving a more realistic experience of the virtual operation, as the surgeon view during cochlear implantation is through a microscope, with various levels of magnification; up to x 32.

The hierarchical data structure of node and field constructs within the Reachin API is suited to event-handling for object manipulation. For visualization and physical representation of objects, surface rendering is applied since the ST walls are constructed of bone and as such do not transform during a live insertion. Assuming that the inside volume that comprises the CI carrier does not deform, variation in the topography of the carrier (such as bending and flexing) as it is inserted into the ST may be modeled with polygonal primitives and/or sample points. Surface representations of the FE ST model, the BM, an approximated Nucleus® 24 Contour electrode and straightening stylet, as well as surgical tweezers were initially constructed in ANSYS and exported as VRML scene graphs, modified for file size reduction without compromise of surface fidelity, and visually rendered in the Reachin API. As described, event-handling was implemented using Python script: which accessed and modified the rotation and translation fields of the objects' transformation nodes to enable real-time rotation and translation of objects rendered within the scene. In effect, changes in model size, rotation and translation can be administered by the user via the keyboard during program execution, such as for arbitrary user movement of the virtual CI and subsequent advancement into the ST model. For this process, the position and orientation fields of the tracker device were routed to translation and rotation fields of the CI, whilst the user presses the haptic device button.

Model optimizations were required in order to achieve system stability and enable real-time user interactions with the surface models. These techniques overcame notable delays in the visual and haptic rendering loops, which were particularly evident during implant/model collisions and often resulted in program termination. The initial representation of the silicone carrier was comprised of many small polygons that were defined within a CollidingController node, within the Reachin API. This geometric model of the carrier was simplified to twelve sample points distributed along the longitudinal axis of the carrier. The sub-sampled CI is of a point-set geometry and is defined within the haptic representation of the CI. The point-set is redefined during collision detection and response as it is interactively advanced into the model. As determined from testing, twelve was the maximum number of points that would provide a stable insertion during CI/ST wall collisions. During sample point distribution, the points were combined with a simplified, visual representation of the carrier end in the Reachin API, as a visual cue for the surgeon. The simplified polygonal representation was produced via polygon decimation and includes the end portion of the carrier with marker ribs, which the surgeon may 'grasp' with the virtual tweezers during a virtual CI insertion.

The visual and haptic models of the ST were optimized; however during this process, the approximations were derived from the same original set of data that defined the FE ST model. The haptic representation of the ST was simplified to reduce the data set size, using polygon reduction. During CI advancement, the sub-sampled carrier interacts with this modified ST haptic model. For the haptic model, 95% polygon reduction was applied to reduce the size of the dataset, although this is not visible to the user (described only for the force model). A separate mesh model is used for the visual representation. The apex data is removed from the haptic model since the carrier will never reach this point in a true insertion. These optimizations were conducted in consideration of the trade-off between real-time simulator

response and structure surface fidelity (for the ST visual, haptic and CI models). The final combination of optimized models provided the best result in terms of haptic responsiveness, structural integrity and system stability.

The stylet and physical representation of the BM are absent from the simulation in order to reduce the file size and processing time to achieve real-time haptic rendering. Future work should include haptic properties of the BM and other structures within the CP, which would involve modeling tissue elasticity properties for these structures. This work focused on the haptic interactions between the CI and ST only.

Dynamic behavior of the model was considered through attributing physical properties obtained via experimentation and from published literature to both the ST and CI representations. The ST was attributed frictional surface properties including those of friction coefficients, stiffness and damping. The attributes for mass, proxy size, stiffness, damping and inertia were provided for haptic model of the sub-sampled carrier. For these properties, values as measured or determined from the literature were assigned that are closest to the in vivo scenario in the absence of quantifiable in vivo measurements or in vitro human data. Values for the ST haptic surface model for friction coefficients were experimentally determined to be: starting as 0.0605 and dynamic 0.0395. These were determined between the silicone carrier and a lubricated Teflon surface. A stopping friction coefficient estimated as 0.0185 was also attributed to the ST model.

Stiffness refers to the capacity of an object to resist a deflection which is caused by an applied force. Damping is a body's ability to reduce the amplitude of its oscillations in order for it to return to rest. To the authors' knowledge, the stiffness of the OC has not been published and it was not possible to determine the value experimentally, so it is approximated as the stiffness of the human footplate (compact ivory bone), published in the literature as 441N/m [42]. In the ST model, normal stiffness is set to this value. Tangential stiffness is estimated as 200N/m. Surface damping is set to 0.01 which is the damping value for the frequency range 1Hz to 100Hz inclusive [43]; since human 'finger' tremor (representative of arm, hand and finger tremor) during object movement is between 1Hz and 30Hz [44], the damping value for the frequency range in [43] is appropriate.

Inertia is a body's ability to resist a change in velocity. An object with a high mass has a high inertia and is more likely to resist acceleration than an object with a low inertia. It is important to define inertia for the carrier, as it may be arbitrarily moved about the scene by the user. The inertia for the silicone carrier is modeled using a BoxInertia applied to the sample points that comprise the carrier for the haptic model. In this dynamic behavior, as the carrier experiences changes in velocity, the points move about the carrier's longitudinal axis and attempt to return to their rest position, in a spring-damper motion. The sample points have stiffness and damping attributes, for linear and rotational movement. The damping value for rotational movement is 0.00003N.m.s/rad and stiffness is 0.2N.m/rad. For linear motion, damping is 1.0N.s/m and stiffness is 350N/m, as documented by Kha et al. [45] for the Contour™ Array stiffness profile. The size of the carrier sample point radius is set to 0.00025m; this is the actual size of the carrier tip as measured from a true Contour™ electrode.

The mass of the carrier is set to be 0.0178943kg, which was measured in the work and includes the combined mass of the actual CI and tweezers. The user would hold the combined mass during a live insertion so this is replicated in the virtual suite (the virtual tweezers were not assigned physical properties). The size parameter representing the boundary conditions for sample point movement is set to 3cm movement in the x-plane, a 2cm movement in the y-plane and a 2cm movement in the z-plane. This parameter needed to be defined since its default value is 0 which does not enable deflection about the centre of gravity.

During CI insertion, there are surface interactions creating between the carrier and the ST walls. Insertion forces caused by these interactions are modeled for the SIT as the virtual carrier is fully inserted into the ST. During an electrode insertion, there are forces acting on the ST walls and electrode which contribute to the total insertion force. These forces include force due to friction between the walls of the ST and CI surface, input force as applied by the user, relaxation force of the CI due to the recoil properties of the pre-curled silicone and adhesion forces. As discussed earlier, net insertion forces and frictional forces were measured via experimentation. The insertion studies provided output force profiles; force output at different stages of CI advancement into the ST chamber, which are compared with similar force profiles generated by the haptic-rendered simulator for system validation (refer Results and Discussion sections). Coefficients of friction as described previously are included as parameters in the force model.

The force model produced in the simulation is based on ST/CI interactions as determined from the insertion studies. In this algorithm, real-time carrier tip position and force output information is logged for each of the three dimensions, to an external data file. The position data is obtained for device position and linear force output. The direction of implant movement is first determined, to see if the electrode is being inserted or withdrawn from the ST. A change in insertion depth occurs if there is a change in displacement of the implant along the z-plane. If the carrier proxy position is greater than the device position the implant is recognized as being inserted into the ST chamber. However if the proxy position is less than the device position, the CI is being withdrawn from the ST representing device movement is along the positive z-plane ('out' of the GUI). If the implant is detected as being inserted into or being removed from the ST, and there is a force detected along the z-plane, the algorithm will consider the contribution of frictional force and is added or subtracted respectively to the z-direction force, in the current force model. The component of frictional force is calculated by obtaining the force acting in the x-plane (perpendicular to the z-plane) and multiplying this force due to friction by the dynamic coefficient of friction (0.0395). The magnitude of the frictional force component is meant to rise as more surface area comes in contact with the ST walls and the

force magnitude decreases for the opposite scenario. As such, during an insertion the algorithm adds the frictional force components to the z-direction force and subtracts the components during an implant withdrawal.

If the force output in the z-direction is non-zero, then the position of the device is considered in order to determine the sample point location. Upon detection of a collision between the ST and carrier in the vicinity of the Basal turn, the algorithm recalculates the carrier sample points which are redefined along the longitudinal carrier axis. These new locations depend on the insertion distance. The sample point number is maintained at its maximum number (12). The additive effect of force due to friction is modeled as the carrier is inserted by adding a force vector as described previously and so the total output force along the z-axis increases as the electrode is fully inserted. Carrier re-sampling facilitates full implantation of the electrode which causes a rise in insertion force along the longitudinal (z-) axis of the carrier.

The final system, showing a virtual implantation during insertion of the force model of the carrier into the haptic surface model of the ST is represented, for the simulator is represented in Fig. 3.

Fig. 3. Simulator Interface for a Haptic-Rendered Virtual Prosthetic Implantation

III. Results

Force profiles over implant displacement along the ST were obtained experimentally and from the simulation, for simulator validation. From the electrode trajectory and force data obtained experimentally, average output values and first standard deviations were calculated from the set of insertion forces. This data is plotted in Fig. 4.

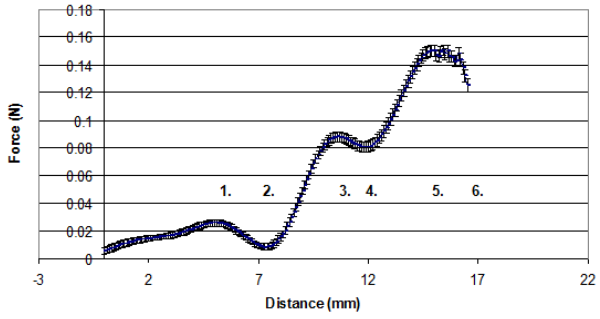

Fig. 4. Average Insertion Force Profile from Experimental Results

As the electrode was inserted into the ST for a SIT, the total force generally increases. There is a small peak at the 4mm distance which is due to the slightly curved outer edge of the carrier hitting the cochleostomy site. After the 5mm mark, as the tip no longer touches the inner wall and the side slides along the outer wall as it progresses to the Basal Turn. There is a peak in insertion force at the point where the electrode touches the Basal Turn, averaging 0.095N, around the 9-12mm depth. Force profiles exhibit an overall continued increase to the average peak value, just before the carrier rib touches the cochleostomy site. After this point, forces increase dramatically and the stylet is then withdrawn.

Haptic-rendered cochlear implantation was performed using the surgical simulator to produce 200 sets of force and position data. The least-squares minimization function is applied to the dataset, to produce a new data series which may be compared with the experimental results. The force and position data represented by the spline are translated along the z-direction a distance of 2.661mm. This value was calculated by considering the location and magnitude of the ST inner and outer wall radii at the RW, as well as the 3mm maximum electrode advancement prior to starting the insertion. It should also be noted that before commencement of the insertion, the ST is rotated 110º to gain a clear view of the ST opening. Once the data is translated 2.661mm, the starting position of the insertion corresponds to a displacement of 0mm, in the z-direction. The data are then sampled at dedicated points along the ST length in 0.1mm increments (with linear interpolation between points). The end result is a set of data points that represent insertion force values from 0mm to 16.5mm, with intervals 0.1mm between sample points. This method is applied for the entire set of results (from 200 tests) produced by the virtual cochlear implantations. This allows for statistical data extraction and comparisons between test results.

All spline data representing insertion forces and relative insertion depth are combined to produce a single spline that represents the average force delivered to the user during a virtual insertion. The average force profile is discussed in relation to electrode position and its physical behaviour for the various stages of an insertion. The first standard deviation is computed and the standard error of the mean is calculated by dividing the standard deviation by the square root of the data count (200). Confidence intervals (95%) are determined about the mean by multiplying the standard error of the mean by 1.96. The average data plotted with the first standard deviations are shown in Fig. 5.

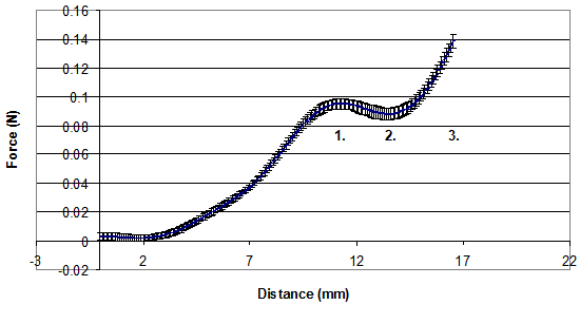

Fig. 5 Average Insertion Force Profile from Simulator Results

As the virtual implant is inserted into the model of the ST, the total force generally increases. Output force rises during CI advancement, as the carrier touches the ST OW and exerts pressure in this region. There is also frictional force contribution as the side of the carrier slides along the outer wall during its advancement towards the Basal turn. Forces increase to an average peak insertion force of 0.095 N (± 0.003 N), at a displacement of 11.2mm. After contact is made at the Basal turn, the output force dips to 0.088N (± 0.004 N) at 13.4mm. As advancement continues past this point, force delivery increases to 0.1389 N (± 0.0047 N) at 16.5mm, which is a total distance of approximately 19.5mm from the cochleostomy site. Insertion can be continued to the maximum depth of 22mm from the cochleostomy site, however the insertions were stopped around 16.5mm from the starting position (1mm to 3mm inside the ST opening). This is the same stopping criterion as the insertions performed in the experimentation.

The same statistical measures were calculated for the experimental data, as for the results produced from the simulation. The force profile for the experimental data is shown in Fig. 4. The overall increase in output force with displacement, as well as locations of peaks and troughs, remain the same. The peak in insertion force around the Basal turn, which corresponds to the electrode tip touching the lateral wall in this region, measures 0.0880N (± 0.0186N) for the Contour array, at distance 10.6mm. The average peak value at the Basal turn was measured previously at 0.095N (± 0.0132N), between 9mm and 12mm. The average peak insertion force for the original data is 0.113N (± 0.0133N), just prior to reaching the peak value of 0.194N (± 0.0287N) where the first marker rib touches. After this point, the force drops off slightly. For the spline approximation, the insertion force increases to a final average peak value of 0.1509N (± 0.0189N) before a slight decrease in output force.

IV. Discussion

The results produced from the spline approximations of the simulation and experimental data are compared, and are represented by Figs. 4 and 5 respectively. For both approximations, the output force generally increases as the distance traversed by the electrode increases, from its starting (0mm) to stopping (16.5mm) position. This distance is measured along the z-axis for the results produced from the simulation. For both sets of results (simulated and experimental), the average output force generally increases to a peak value around the Basal turn: 0.095N (± 0.003N) at a displacement of 11.2mm for the simulation results and 0.0880N (± 0.0186N) at 10.6mm for experimental results. For the results produced from the experimentation, there is a small peak around the 6mm mark and a dip around the 8mm mark. The force then increases to a peak at the Basal turn. The results produced by the simulations do not show the same dramatic changes about this region. After the Basal turn region, both force profiles exhibit a dip in output force: 0.088N (± 0.004N) at 13.4mm for the simulation results and 0.0807N (± 0.0219N) at 11.8mm for the experimental results. After this point, forces increase in both scenarios to a value of to 0.1389N (± 0.0047N) at 16.5mm for the simulation results and 0.1509N (± 0.0189N) at 15.4mm for the experimental results. After reaching a maximum value of 0.1509N, the force output for the experimental results decreases to 0.1254N (± 0.0385N) at 16.5mm.

A. Validation of the Simulator

The haptic simulator may be validated by determining the degree of similarity between the force profile results obtained experimentally and those produced from the simulation. Any anomalies may be explained with reference to the insertion process. The average force values from Fig. 5 are subtracted from the average force values in Fig. 4 to give the difference between mean simulator and experimental results, for each 0.1mm interval from 0mm to 16.5mm. The difference in the standard error of the mean is calculated and upper as well as lower confidence intervals (95%) are then derived (Fig. 6).

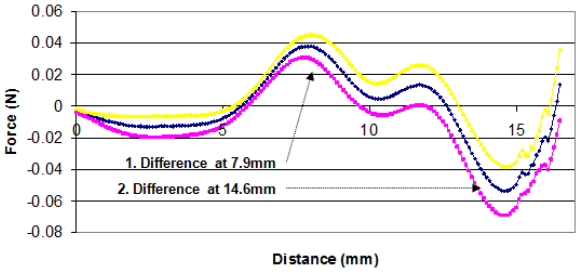

Fig. 6 Difference in Force Insertion Data between Experimentation and Simulation Results

From the results, confidence levels are analyzed to examine any variation about 0N and likely causes for such variation. Differences in average forces and the respective confidence intervals may be evaluated in terms of statistical significance and practical importance. Inaccurate force reflection provided by a simulator means that force delivery is misrepresentative of the true scenario and may have an impact on administration technique. Practical implications due to misrepresentation of the true scenario for this type of application, for the ENT surgeon could lead to excessive force administration causing damage to the implant or delicate ST structures.

As the electrode is inserted into the ST from 0mm to 5mm, the difference reaches -0.01285N at 2.5mm. At this point, there is a 95% confidence that the difference is no less than -0.0196N and no greater than -0.0061N. Differences in this region can be attributable to the carrier shape: in the simulation the carrier is sub-sampled by spheres of uniform geometry, centred on the longitudinal axis of the carrier which is linear. However, in the experimentation, the carrier form may be slightly curved and is tapered. As the carrier is inserted, its outer side touches the cochleostomy site and creates a change in force profile at this point. In effect, force output changes due to a difference in ST/CI interactions between the two scenarios.

The difference between the force magnitudes decreases to 0N at an insertion displacement of about 5.6mm and there is a

95% confidence that the difference will be no less than -0.0035N and no greater than 0.0043N. This means that at this stage where the carrier is sliding along the outer ST wall at a distance of 5.6mm, the force output from the simulator is equal to the force output in the experimentation. Just before the electrode reaches the Basal turn region, the difference increases to a peak value of 0.0380N at 7.9mm, where there is a 95% confidence that the difference in output forces will be no less than 0.0306N and no greater than 0.0454N. In the experimental results, there is a dip in output force at this point due to the carrier tip no longer making contact with the ST IW. The tip should, under ideal conditions, rest against the outer wall since the carrier design with the stylet in place is straight. However, in practice a slight curvature in carrier design was observed during insertion tests, which was not replicated in the simulation. The silicone curvature could be caused by human or mechanical influences, most likely the stylet is not fully inserted into its silicone envelope, or deformation of the stylet and/or carrier where either or both are slightly bent. The tendency of the silicone carrier to assume its pre-curled state may add to this effect.

The difference decreases to 0.0046N at 10.3mm, with a 95% confidence that the difference will have a minimum value of -0.0056N and a maximum of 0.0148N. This position corresponds to the location of the Basal turn, in the proximity where the tip would touch the lateral outer wall of the ST. Here, variation is close to 0N and the confidence intervals include 0N, indicating that at the Basal turn, the simulation closely represents the physical interactions that occur between the electrode and ST walls in the insertion experiments. After the Basal turn region, there is a slight increase in the difference to 0.0135N at 11.7mm, with 95% confidence limits of 0.0005N and 0.0264N. The difference returns to 0N at 12.6mm. As the electrode displacement increases to 14.6mm, the difference in average reaches -0.0536N, where the force output from the simulation exceeds the experimental average with a 95% confidence interval of -0.0693N to -0.0380N. The difference returns to 0N just after a 16.3mm displacement, where the electrode is close to its full insertion depth. At full insertion depth (16.5mm) the difference is 0.0135N, yet the confidence limits, -0.0093N and 0.0363N, reveal that at full carrier displacement the difference is not statistically significant.

For regions that are statistically significant (the confidence intervals do not include 0N), the difference in average output force does not exceed 0.0536N in magnitude. As reported in the literature, a human can distinguish the difference between two forces if there is a variation in force magnitude of 0.5N [44]. Since the greatest difference in the magnitude of force between the simulator and experimental results is 0.0536N, this variation could not be tactically detected by the user. As such, although these regions are statistically significant, they are of no practical importance for differentiation of haptic feedback.

Differences of less than 0.0536N may however have other practical implications for this type of surgery. These may include excessive force administration that may affect the physical characteristics of the implant and/or cochlear structures. This degree of force variation might affect the position and dynamic behavior of the implant, such as a change in magnitude of its deflection during contact with the ST walls, or may induce varying degrees of damage to soft tissue structure (such as the Osseous Spiral Lamina (OSL) or BM) during a live implantation. Further investigation must be conducted to determine the magnitude of force administration that will directly cause damage to these cochlear structures since it is currently not reported in the literature.

V. Conclusion

A real-time haptic-rendered surgical simulator has been produced in the work to enable the prosthetic insertion of a virtual Cochlear Implant (CI), for surgeon training and pre-operative planning. Insertion studies were conducted to evaluate implant behavior and quantify insertion forces during electrode advancement into a synthetic model of the ST. As the next stage in simulator design, a parametric model of the ST was derived from measured data. Surface model optimizations were performed to enable real-time model interactions. Visual and force rendering algorithms were designed and developed, based on the insertion studies conducted in the work. During program execution, the user is able to interact with the VE using the haptics device, to arbitrarily insert the virtual implant into the ST model. As the user performs the real-time, virtual insertion, forces are delivered back to the user through the haptic interface. The force delivery of the sub-sampled Contour™ array is modeled for the Standard Insertion Technique (SIT). Other techniques including the Advance-Off Stylet (AOS) insertion have not been simulated. Simulator accuracy is validated by quantitatively comparing the results from the simulation with those obtained experimentally, from the insertion studies. Future work may include representation of the BM as a soft tissue structure, simulating surface deformations and puncturing, construction of the Scala Vestibuli (SV) as a secondary passage for CI insertion and enabling the user to perform other insertion techniques (such as the AOS insertion method), with the option to use other manufacturer implant designs.

References

[1] B. Pflesser, A. Petersik, U. Tiede, K. H. Hohne and R Leuwer, "Volume cutting for virtual petrous bone surgery," *Computer Aided Surgery*, vol. 7, pp. 74-83, 2002.

[2] J. Wiet, D. Stredney, D. Sessanna, J. A. Bryan, D. B. Welling and P. Schmalbrock, "Virtual temporal bone dissection: an interactive surgical simulator," *Otolaryngology - Head and Neck Surgery*, vol. 127, pp. 79-83, 2002.

[3] A. Petersik, B. Pflesser, U. Tiede, K. H. Hohne and R. Leuwer, "Realistic haptic interaction in volume sculpting for surgery simulation," *Surgery Simulation and Soft Tissue Modeling, International Symposium (IS4TH 2003)*, pp. 194-202, 2003.

[4] W. John, N. Thacker, M. Pokric, *et al.*, "An integrated simulator for surgery of the petrous bone," *Medicine Meets Virtual Reality 2001*, pp. 218-224, 2001.

[5] M. Agus, A. Giachetti, E. Gobbetti, G. Zanetti and A. Zorcolo, "Real-time haptic and visual simulation of bone dissection," *Presence*, vol. 12, pp. 110-122, 2003.

[6] M. Hutchins, S. O'Leary, D. Stevenson, C. Gunn and A. Krumpholz., "A networked haptic virtual environment for teaching temporal bone surgery," *Medicine Meets Virtual Reality (MMVR) 13*, pp. 204-207, 2005.

[7] A. Pommert, K. H. Höhne, E. Burmester, S. Gehrmann, R. Leuwer, A. Petersik, B. Pflesser and U. Tiede, "Computer-based anatomy: a prerequisite for computer-assisted radiology and surgery," *Academic Radiology*, vol. 13, pp. 104-112, 2006.

[8] Kim, S. De and M. A. Srinivasan, "Computationally efficient techniques for real time surgical simulation with force feedback," *Proceedings of the 10th Symp. On Haptic Interfaces for Virtual Envir. & Teleoperator Systs. (Haptics '02)*, pp. 51-57, 2002.

[9] G. Burdea, G. Patounakis, V. Popescu and R. E. Weiss, "Virtual reality-based training for the diagnosis of prostate cancer," *IEEE Transactions on Biomedical Engineering*, vol. 46, pp. 1253-1260, 1999.

[10] A. Chanda and T. Kesavadas, "Real-time volume haptic rendering of non-linear viscoelastic behavior of soft tissue through dynamic atomic unit approach," *Medicine Meets Virtual Reality 12*, Newport Beach, California, pp. 16-17, 2004.

[11] Y. Kuroda, M. Nakao, T. Kuroda, H. Ovama and M. Komori, "Interaction model between elastic objects for haptic feedback considering collisions of soft tissue," *Computer Methods and Programs in Biomedicine*, vol. 80, pp. 216-224, 2005.

[12] Y.-J. Lim and S. De, "Nonlinear tissue response modeling for physically realistic virtual surgery using PAFF," *First Joint Eurohaptics Conference and Symposium on Haptic Interfaces for Virtual Environment and Teleoperator Systems (WHC 2005)*, pp. 479-480, 2005.

[13] M. O. Alhalabi, V. Daniulaitis, H. Kawasaki and T. Hori, "Medical training simulation for palpation of subsurface tumor using HIRO," *First Joint Eurohaptics Conference and Symposium on Haptic Interfaces for Virtual Environment and Teleoperator Systems (WHC 2005)*, pp. 623-624, 2005.

[14] S. P. DiMaio and S. E. Salcudean, "Interactive simulation of needle insertion models," *IEEE Transactions on Biomedical Engineering*, vol. 52, pp. 1167-1179, 2005.

[15] K.-U. Kyung, D.-S. Kwon, S.-M. Kwon, H. S. Kang and J. B. Ra, "Force feedback for a spine biopsy simulator with volume graphic model," *IEEE International Conference on Intelligent Robots and Systems*, pp. 1732-1737, 2001.

[16] E. Gobbetti, M. Tuveri, G. Zanetti and A. Zorcolo, "Catheter insertion simulation with co-registered direct volume rendering and haptic feedback," *Medicine Meets Virtual Reality 2000 - Envisioning Healing: Interactive Technology and the Patient-Practioner Dialogue*, pp. 96-98, 2000.

[17] X. Wang and A. Fenster, "A virtual reality based 3D real-time interactive brachytherapy simulation of needle insertion and seed implantation," *IEEE International Symposium on Biomedical Imaging: Macro to Nano*, pp. 280-283, 2004.

[18] P.-A. Heng and T.-T. Wong, "Intelligent inferencing and haptic simulation for chinese acupuncture learning and training," *IEEE Transactions on Information Technology in Biomedicine*, pp. 1-1, 2005.

[19] F. P. Vidal, N. Chalmers, D. A. Gould, A. E. Healey and N. W. John, "Developing a needle guidance virtual environment with patient-specific data and force feedback," *International Congress Series*, vol. 1281, pp. 418-423, 2005.

[20] W. Chou and T. Wang, "Human-computer interactive simulation for the training of minimally invasive neurosurgery," *IEEE International Conference on Systems, Man and Cybernetics*, pp. 1110-1115, 2003.

[21] P. Gorman, T. Krummel, R. Webster, M. Smith and D. Hutchens, "A prototype haptic lumbar puncture simulator," *Medicine Meets Virtual Reality (MMVR)*, pp. 106-109, 2000.

[22] A. Zorcolo, E. Gobbetti, G. Zanetti and M. Tuveri, "A volumetric virtual environment for catheter insertion simulation," *Virtual Environments 2000, Proceedings of the Eurographics Workshop*, Amsterdam, the Netherlands, 2000.

[23] Aloisio, L. Barone, M. Bergamasco, C. A. Avizzano, L. T. De Paolis, M. Franceschini, A. Mongelli, G. Pantile, L. Provenzano and M. Raspolli, "Computer-based simulator for catheter insertion training," *Medicine Meets Virtual Reality 12*, pp. 4-6, 2004.

[24] M. Brahim and Y. Amirat, "Interactive navigation control with haptic rendering of endovascular treatment," *IEEE Conference on Robotics, Automation and Mechatronics*, pp. 60-64, 2004.

[25] D. d'Aulignac, R. Balaniuk and C. Laugier, "A haptic interface for a virtual exam of the human thigh," *IEEE International Conference on Robotics and Automation (ICRA)*, pp. 2452-2457, 2000.

[26] U. Kühnapfel, H. K. Çakmak and H. Maaß, "Endoscopic surgery training using virtual reality and deformable tissue simulation," *Computers & Graphics*, vol. 24, pp. 671-682, 2000.

[27] G. Gopalakrishnan and V. Devarajan, "StapSim: A virtual reality-based stapling simulator for laparoscopic herniorrhaphy," *Medicine Meets Virtual Reality 12*, Newport Beach, California, pp. 111-113, 2004.

[28] C. Basdogan, C.-H. Ho and M. A. Srinivasan, "Virtual environments for medical training: graphical and haptic simulation of laparoscopic common bile duct," *IEEE/ASME Transactions on Mechatronics*, vol. 6, pp. 269-285, 2001.

[29] Zhang 2004 H. Zhang, S. Payandeh, J. Dill and A. J. Lomax, "Acquiring laparoscopic manipulative skills: a virtual tissue dissection training module," *Medicine Meets Virtual Reality 12*, pp. 419-421, 2004.

[30] C. Gunn, M. Hutchins, M. Adcock and R. Hawkins, "Surgical training using haptics over long internet distances," *Medicine Meets Virtual Reality 12*, pp. 121-123, 2004.

[31] M. P. Ottensmeyer, E. Ben-Ur and J. K. Sailsbury, "Input and output for surgical simulation: devices to measure tissue properties in vivo and a haptic interface for laparoscopy simulators," *Medicine Meets Virtual Reality*, pp. 236-242, 2000.

[32] H. Maaß, H. Çakmak, U. Kühnapfel, C Trantakis and G. Strauss, "Providing more possibilities for haptic devices in surgery simulation," *International Congress Series*, vol. 1281, pp. 725-729, 2005.

[33] M. Bro-Nielsen, D. Helfrick, B. Glass, X. Zeng and H. Connacher, "VR simulation of abdominal trauma surgery," Medicine Meets Virtual Reality (MMVR), pp. 117-123, 1998.

[34] B. K. Chen, G. M. Clark and R. Jones, "Evaluation of trajectories and contact pressures for the straight nucleus cochlear implant electrode array - a two-dimensional application of finite element analysis," *Medical Engineering & Physics*, vol. 25, pp. 141-147, 2003.

[35] S. K. Yoo, G. Wang, J. T. Rubinstein and M. W. Vannier, "Three-dimensional geometric modeling of the cochlea using helico-spiral approximation," *IEEE Transactions on Biomedical Engineering*, vol. 47, pp. 1392-1402, 2000.

[36] D. R. Ketten, M. W. Skinner, G. Wang and M. W. Vannier, "In vivo measures of cochlear length and insertion depth of nucleus cochlear implant electrode arrays," *Annals of Otology, Rhinology & Laryngology*, vol. 107, pp. 1-16, 1998.

[37] L. T. Cohen, J. Xu, S. A. Xu and G. M. Clark, "Improved and simplified methods for specifying positions of the electrode bands of a cochlear implant array," *The American Journal of Otology*, vol. 17, pp. 859-865, 1996.

[38] A. Kawano, H. L. Seldon and G. M. Clark, "Computer-aided three-dimensional reconstruction in human cochlear maps: measurement of the lengths of organ of corti, outer wall, inner wall, and rosenthal's canal," *Annals of Otology, Rhinology & Laryngology*, vol. 105, pp. 701-709, 1996.

[39] J. T. Vrabec, S. W. Champion, J. D. Gomez, R. F. Johnson Jr, G. Chaljub, "3D CT imaging method for measuring temporal bone aeration", *Acta Oto-Laryngologica*, vol. 122, no. 8, pp. 831-835, 2002.

[40] E. Givelberg and J. Bunn, "Computational experiments with a three-dimensional model of the cochlea," Technical Report, California Institute of Technology, Caltech CACR, 2004.

[41] S.-I. Hatsushika, R. K. Shepherd, Y. C. Tong, G. M. Clark and S. Funasaka, "Dimensions of the scala tympani in the human and cat with reference to cochlear implants," *Annals of Otology, Rhinology & Laryngology*, vol. 99, pp. 871-876, 1990.

[42] H. M. Ladak, "Finite-element modelling of middle-ear prostheses in cats", *Masters Thesis*, Montreal, Canada, McGill University, 1993.

[43] R. Lakes, H. S. Yoon and J. L. Katz, "Ultrasonic wave propagation and attenuation in wet bone," *Journal of Biomedical Engineering*, vol. 8, pp. 143-148, 1986.

[44] J. Raethjen, F. Pawlas, M. Lindemann, R. Wenzelburger and G. Deuschl, "Determinants of physiologic tremor in a large normal population," *Clinical Neurophysiology*, vol. 111, pp. 1825-1837, 2000.

[45] H. N. Kha, B. K. Chen, G. M. Clark and R. Jones, "Stiffness properties for nucleus standard straight and contour electrode arrays," *Medical Engineering & Physics*, vol. 26, pp. 677-685, 2004.

Catherine A. Todd (M'09) Member (SM) graduated from the University of Wollongong, Australia, with a PhD in Electrical Engineering, in 2006 and a Bachelor in Electrical Engineering, Honors Class I in 2002. Catherine has been an Assistant Professor in Computer Science and Engineering at the University of Wollongong in Dubai, UAE, since 2006. Catherine's research specialization is in surgical simulation for artificial hearing applications.

She undertook an engineering cadetship at BHP Steelworks Port Kembla, Australia, from 1997 to 2002, working full-time as a BHP Electrical Engineering Degree Cadet. From 2002 to 2006 she worked part-time as a casual academic staff member at the University of Wollongong, Australia, while undertaking her PhD. Current research interests are in biomedical engineering, medical image processing and control applications, specifically virtual reality modeling and simulation of middle and inner ear anatomy and associated clinical interventions.

Dr. Todd is a reviewer for the Journal of Computer Assisted Radiology and Surgery. Catherine won a best paper award at the JCMIT conference 2009 and has won several research grants, including the top category award for the National Research Foundation (NRF) 2009 UAE grants.

Fazel Naghdy (M'02) received his first degree from Tehran University in 1976, MSc and PhD from the Postgraduate School of Control Engineering, University of Bradford, England, in 1979, 1982 respectively.

He is currently a Professor University of Wollongong, School of Electrical, Computer & Telecommunications Engineering, Australia. He is also Director of the Center for Intelligent Mechatronics Research. His current research interests include haptic rendered virtual manipulation of clinical and mechanical systems, intelligent control and learning in non-linear and non-structured systems.

Fazel has served on a large number of International scientific committees of various international conferences. He is a contributing editor to the IEEE Transactions on Mechatronics Engineering, International Journal of Intelligent Automation and Soft Computing and has more than 250 publications in international journals and conferences and as book chapters.